In-plane topological p-n junction in the three-dimensional topological insulator Bi$_{2-x}$Sb$_x$Te$_{3-y}$Se$_y$

Ngoc Han Tu[1], Yoichi Tanabe[1], Yosuke Satake[1], Khuong Kim Huynh[2] & Katsumi Tanigaki[1,2]

A topological p-n junction (TPNJ) is an important concept to control spin and charge transport on a surface of three-dimensional topological insulators (3D-TIs). Here we report successful fabrication of such TPNJ on a surface of 3D-TI Bi$_{2-x}$Sb$_x$Te$_{3-y}$Se$_y$ thin films and experimental observation of the electrical transport. By tuning the chemical potential of n-type topological Dirac surface of Bi$_{2-x}$Sb$_x$Te$_{3-y}$Se$_y$ on its top half by using tetrafluoro-7,7,8,8-tetracyanoquinodimethane as an organic acceptor molecule, a half surface can be converted to p-type with leaving the other half side as the opposite n-type, and consequently TPNJ can be created. By sweeping the back-gate voltage in the field effect transistor structure, the TPNJ was controlled both on the bottom and the top surfaces. A dramatic change in electrical transport observed at the TPNJ on 3D-TI thin films promises novel spin and charge transport of 3D-TIs for future spintronics.

[1] Department of Physics, Graduate School of Science, Tohoku University, 6-3 Aramaki, Aoba-ku, Sendai, Miyagi 980-8577, Japan. [2] WPI-Advanced Institute for Materials Research, 2-1-1 Katahira, Aoba-ku, Sendai, Miyagi 980-8578, Japan. Correspondence and requests for materials should be addressed to Y.T. (email: ytanabe@m.tohoku.ac.jp) or to K.T. (email: tanigaki@sspns.phys.tohoku.ac.jp).

Three-dimensional topological insulators (3D-TIs)[1,2] provide a new platform for research on electronic properties in materials science. Their helical spin-locked Dirac-cone surface states[3,4] are ideal for ultralow dissipative electrical transport, which includes both spin and charge degrees of freedom, and a new design of a logical circuit applicable to various electronic devices can be considered[5–14]. One of the most important features for utilizing such intriguing spin-locked surface states is the topological p-n junction (TPNJ)[7–9]. Theoretically, the inverted helical spin structure in contact between p-type and n-type Dirac cones can bring about superior rectification of spin and charge current. For instance, a significantly large backward scattering of charge current at TPNJ can theoretically give rise to current rectification switching as well as amplification in spin current associated with spin polarization[8]. Such TPNJ studies were recently made for graphene[15–17], where pseudo-spin locking is realized via its special geometrical structure and inversion symmetry. Although intensive challenges for fabrication and observation of TPNJs have so far been made also for 3D-TIs as a real spin-locked system[18–22], the important backward scattering and its on–off switching of charge current flow originating from the spin-locked helical Dirac cone surface states have not yet experimentally been reported. Considering the novel electric transport for TPNJ as well as its applications to 3D-TI devices by using ultralow dissipative spin and charge current, truly firm confirmation and understanding on TPNJ fabricated on the in-plane surface of 3D-TIs are very much warranted.

In this letter, we report a fabrication of TPNJ on a surface of single-crystal 3D-TI $Bi_{1.5}Sb_{0.5}Te_{1.7}Se_{1.3}$ (BSTS)[23–27] ultrathin films. For making the TPNJ without less damage on the surface states, we use tetrafluoro-7,7,8,8-tetracyanoquinodimethane (F4-TCNQ), an organic molecule known to provide holes to the Dirac fermion surface states of BSTS[28–31] for tuning the chemical potential on its half from n-type to p-type so that a TPNJ can be created on the in-plane surface as shown in Fig. 1. Because of both a variety of work functions available from organic semiconductors and a simple and non-damaging fabrication process involved in the present methodology[28–31], tuning of carrier type on the 3D-TI surface by using an organic semiconductor molecule via interface contact with 3D-TIs is promising for making TPNJs to observe the intrinsically emerging electrical transport properties. Although the TPNJ is created on the top surface of BSTS thin films, the bottom surface with originally n-type is also modified by the influence of the substrate contact and its chemical potential is further changed under the deposition region of F4-TCNQ. We control the chemical potential of the bottom surface by using back-gating voltage (V_G) in a field effect transistor structure on a SiO_2/Si substrate. We clearly observe a dramatic change in electrical transport by changing the V_G and give an experimental clue so far for the highly coveted TPNJ in connection with the theoretical prediction.

Results

Design of topological p-n junction device. To clarify the electrical transport of TPNJ made on 3D-TIs BSTS, tuning the chemical potential of its topological surface states with keeping the insulating properties of the bulk is essential. BSTS ultrathin films grown on mica followed by transfer to a SiO_2/Si substrate can preserve both their high mobility topological surface states and good insulating bulk electronic states[23–27], and are therefore considered to be the best candidate to manipulate the intrinsic electrical transport of TPNJ. Although a tunable Fermi level from n- to p-type in 3D-TIs has been demonstrated for constructing TPNJ[19,21], intrinsic electric transport experiments for demonstrating TPNJ have not yet been achieved. To tune the chemical potential, we used an organic semiconductor F4-TCNQ, known to be a good electron acceptor, on the BSTS surface. This modification can realize conversion of the n-type topological surface of an as-grown sample with the stoichiometry of $Bi_{1.5}Sb_{0.5}Te_{1.7}Se_{1.3}$ to the p-type one via electron transfer from BSTS to F4-TCNQ owing to its strong electron affinity
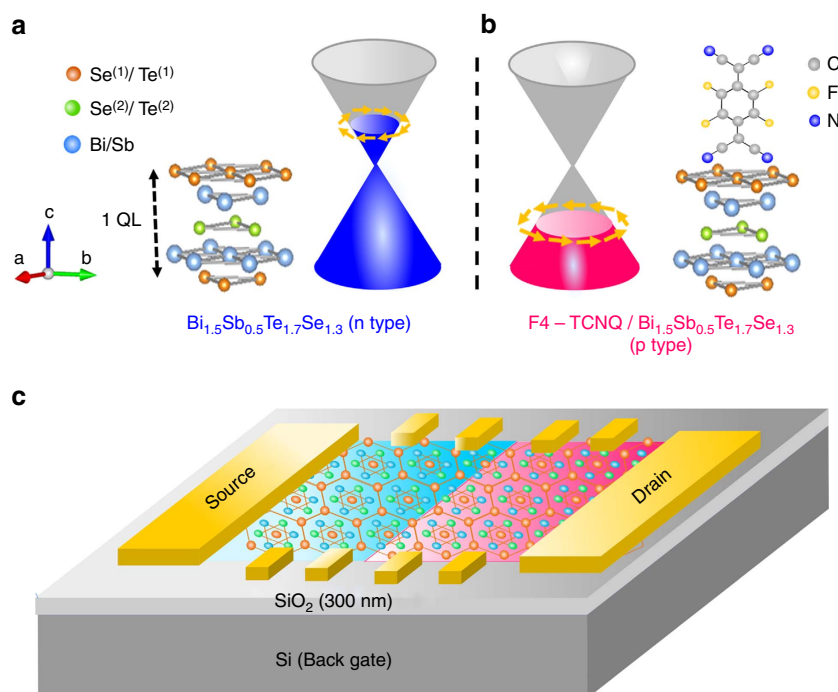

Figure 1 | Schematic view of TPNJ device. (**a,b**) Electronic structure of BSTS and F4-TCNQ/BSTS and (**c**) topological p-n junction device. To make a local carrier tuning on the 3D-TI thin film, F4-TCNQ molecules are partly deposited on the n-type BSTS thin film surface.

(5.24 eV (ref. 32)) with almost no mechanical and thermal damage thanks to the low temperature process (∼60 °C) as well as the π-orbital soft contact as shown in Fig. 1b.

Electrical transport of topological p-n junction device. Figure 2b showed an evolution of four probe resistance (R_{xx}) across the TPNJ made on the top surface between pristine BSTS (n-type surface) and F4-TCNQ/BSTS (p-type surface) as a function of V_G (also see Supplementary Figs 1 and 2 and Supplementary Notes 1 and 2). In the range of V_G between -90 and -30 V, where TPNJ states can be created both on the top and the bottom surfaces as explained later based on the detailed electrical transport properties. R_{xx} showed a markedly abrupt and step-like jump at two particular gate voltages: from 12 to 18 kΩ at $V_G = -30$ V and from 14 to 28 kΩ at $V_G = -90$ V. The high resistance values in this window can be compared with greatly lower resistance of ∼7 kΩ at the V_G positively larger than $+20$ V (n/n contact at the interface both on the top and on the bottom) and ∼12 kΩ at the V_G negatively smaller than -130 V (p/p contact at the interface both on the top and on the bottom), where no TPNJ at the interface between BSTS and F4-TCNQ/BSTS is created. Importantly, no clear difference was experimentally observed between forward and backward bias voltage, being greatly different from the conventional diode properties, reflecting the zero gap linear energy dispersion in 3D-TIs (also see Supplementary Note 3). A clear enhancement in R_{xx} observed in the TPNJ in the FET structure indicated that the spin-locked topological p-n junction strongly scatters electron transmission, which was theoretically expected.

Electrical transport of pristine BSTS and F4-TCNQ/BSTS devices. To clarify the observed TPNJ phenomenon more definitively, useful information was collected on the electrical transport properties for both pristine BSTS and F4-TCNQ/BSTS. Figure 3a shows Hall resistance (R_{yx}) of pristine BSTS and F4-TCNQ/BSTS on mica as a function of magnetic field (**B**). Clear experimental evidence was observed, showing that an n-type negative slope (blue colour) for pristine BSTS was changed to a p-type positive slope (red colour) for F4-TCNQ/BSTS. Longitudinal resistance (R_{xx}) of both pristine BSTS

(blue colour) and F4-TCNQ/BSTS (red colour) is also shown in Fig. 3b as a function of **B**. A convex-like shaped magnetoresistance (R_{xx}) is displayed, showing a typical weak-antilocalization for a spin-momentum-locked metallic surface[33]. Importantly, one can clearly see Shubnikov–de Haas (SdH) oscillations superimposed on the R_{xx}. After calculations of the longitudinal and the transverse conductance G_{xx} and G_{xy} using R_{xx} and R_{yx} as shown in Supplementary Fig. 3a,b, the oscillatory parts of G_{xx} (ΔG_{xx}) and R_{xx} (ΔR_{xx}) were separately extracted as a function of **B** as shown in Fig. 3c,d by subtracting the background using a polynomial function (also see Supplementary Note 4). The amplitude of the oscillations modulated with periodicity of 1/**B** and its decrease in intensity as a function of 1/**B** are consistent with the consequence of the SdH oscillations.

The fact that the oscillation periodicity was clearly different between pristine BSTS and F4-TCNQ/BSTS gives important experimental evidence that the chemical potential was greatly modified by the charge transfer occurring at the interface between BSTS and F4-TCNQ. Via fast Fourier transformation (FFT), two and three oscillation periodicities were estimated to be **B** = 16.7 T and 43.3 T for pristine BSTS and **B** = 3.55 T, 5.95 T and 14.5 T for F4-TCNQ/BSTS, respectively (see Supplementary Fig. 3 and Supplementary Note 4). Note that F4-TCNQ molecules make an action as additional scattering centers as well as an electron acceptor on the surface of 3D-TIs, whereas the previous report of transition metal phtalocyanine molecules act as an electron donor with absence of backward scattering[34,35]. As shown in Supplementary Fig. 4 (also see Supplementary Note 5), pristine BSTS showed a metallic temperature dependence in a wide temperature range, whereas the F4-TCNQ/BSTS showed a more insulting-like behaviour as well as higher resistance than that of pristine BSTS. These suggest that F4-TCNQ molecules may give additional scattering, resulting in the suppression of the carrier mobility in the F4-TCNQ/BSTS device.

In SdH, the resistance can periodically be modulated by

$$\Delta G_{xx} \, \alpha \cos\left[2\pi\left(\frac{F}{B} - \gamma\right)\right] \qquad (1)$$
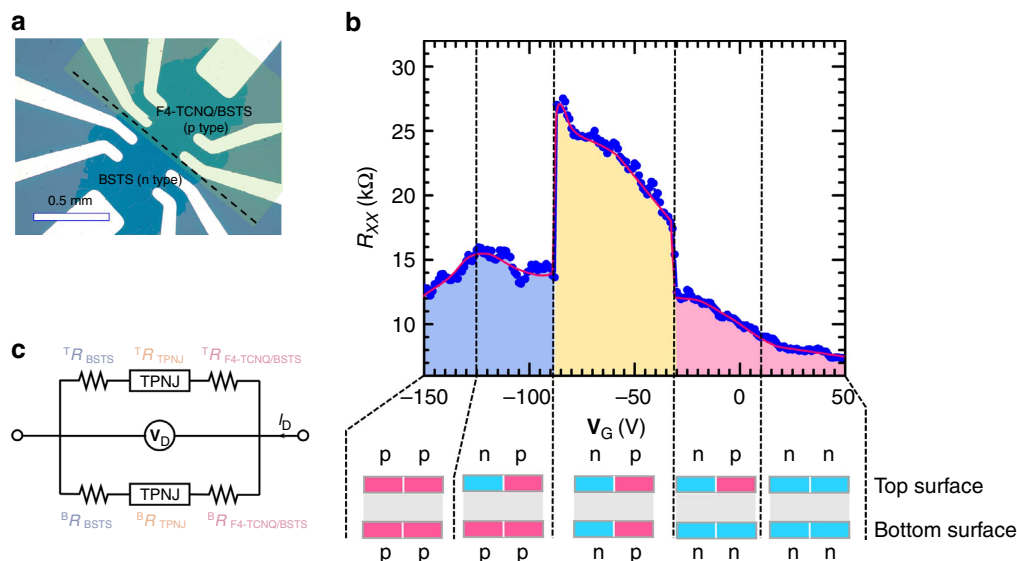

Figure 2 | Electric transport of TPNJ device. (**a**) Microscope view of a TPNJ device. BSTS thin film with 10 nm thickness grown on mica was transferred on a SiO₂/Si substrate to fabricate a bottom gate field effect transistor. F4-TCNQ was partly deposited on the BSTS thin film to realize injection of holes on the partial area of BSTS. (**b**) Gate voltage (V_G) dependence of R_{xx} across the TPNJ made between pristine BSTS and F4-TCNQ/BSTS at 2 K. Schematic views of the TPNJ for the top and the bottom surface states available from the present device are illustrated. (**c**) The equivalent electric circuit of the present device. The electronic circuit of TPNJ involving both top and bottom surfaces can be described as a parallel circuit connection of resistance.
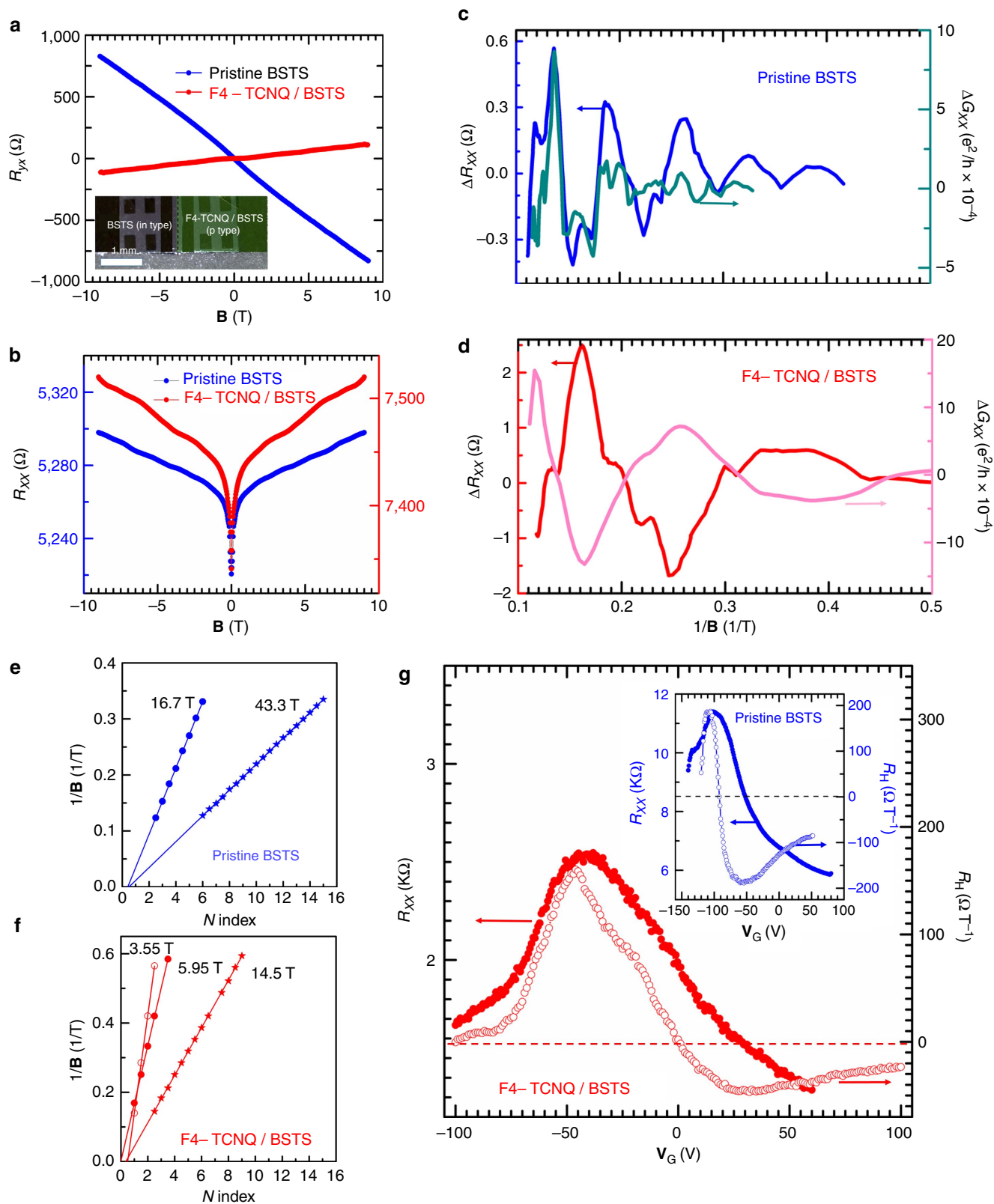
Figure 3 | Electric transport of BSTS and F4-TCNQ/BSTS device. (**a**,**b**) Magnetic field (**B**) dependence of transverse and longitudinal resistance (R_{yx} and R_{xx}) at 2 K for pristine BSTS and F4-TCNQ/BSTS on mica. Inset of **a** shows a microscope view of pristine BSTS and F4-TCNQ/BSTS device. (**c**,**d**) 1/**B** dependence of the oscillatory parts of longitudinal resistance (ΔR_{xx}) and longitudinal conductance (ΔG_{xx}) at 2 K. (**e**,**f**) A Landau level fan diagram plot, where the valley (the peak) in ΔG_{xx} indicates as an integer n (a half integer $n+1/2$). (**g**) Gate voltage (**V**$_G$) dependence of R_{xx} and Hall coefficient (R_H) calculated from R_{yx} at **B** = ± 9 T for a F4-TCNQ/BSTS bottom gate field effect transistor (FET) prepared on a SiO$_2$/Si substrate. Inset shows **V**$_G$ dependence of R_{xx} and R_H for a device for pristine BSTS.

where F/B is the oscillation frequency and γ is the phase factor. The conventional parabolic energy dispersion gives $\gamma = 1/2$, whereas additional $\alpha = 1/2$ originating from the π Berry phase channels[24] is added to $\gamma = 1/2$ in the case of nontrivial topological surfaces. In the Landau level (LL) fan diagram plot, the valley (the peak) in ΔG_{xx} corresponding to an integer n (a half integer of $n + 1/2$) was plotted to deduce further accurate information (Fig. 3e,f)[36,37]. Consequently $\alpha \sim 0.5$ ($\mathbf{B} = 16.7\,\mathrm{T}$ and $43.3\,\mathrm{T}$) for pristine BSTS and $\alpha \sim 0.5$ ($\mathbf{B} = 3.55\,\mathrm{T}$ and $14.5\,\mathrm{T}$); $\alpha \sim 0$ ($\mathbf{B} = 5.95\,\mathrm{T}$) for F4-TCNQ/BSTS (also see Supplementary Figs 3 and 5 and Supplementary Note 4). It is noted that trivial carriers ascribed to the surface accumulation layer were also reported in the case of p-type bulk BSTS[21]. Formation of the Rashba-split quantum-well state was also reported at the interface between phthalocyanine and Bi_2Se_3 owing to the strong band bending and the charge transfer to Bi_2Se_3 (ref. 38). However, Rashba quantum-well states give the π Berry phase[39], and their contribution contradicts with the result of the fan diagram plot and the analysis of the magnetoconductance (see Supplementary Fig. 6 and Supplementary Note 3).

Owing to the influence of a substrate, topological surface states are known not to be identical between the top and the bottom surfaces[40]. For the purpose of having accurate information on both surface states, an FET device with a bottom gate ($\mathbf{V}_G$) was used. Longitudinal resistance (R_{xx}, closed symbols) and Hall coefficient (R_H, open symbols) are displayed as a function of $\mathbf{V}_G$ in Fig. 3g. The existence of the top and the bottom topological surface is clearly recognized as the two transitions displaying a shoulder around at $\mathbf{V}_G = -30\,\mathrm{V}$ in both R_{xx} and R_H for F4-TCNQ/BSTS. The nearly $R_H = 0$ at $\mathbf{V}_G = 0$ observed for F4-TCNQ/BSTS is the consequence of compensation of the Hall voltage between holes and electrons and indicates that the top surface becomes p-type by the F4-TCNQ modification with leaving the bottom surface still as an n-type, owing to the stronger charge transfer from BSTS to F4-TCNQ on the top surface than that on the bottom surface. When positive $\mathbf{V}_G$ is applied, the sign of R_H becomes negative towards a minimum and turns back to zero with keeping its negative sign, indicating that the both surface states can finally become n-type with increasing the number of electron carriers. On the other hand, when negative $\mathbf{V}_G$ is used, the R_H becomes positive first in sign and approaches towards a maximum followed by returning back to a small value with preserving the same sign for both pristine BSTS and F4-TCNQ/BSTS. Accordingly, in the negative $\mathbf{V}_G$ limit, both top and bottom topological surfaces can be tuned to be p-type. The intriguing sign change can be observed in the middle range from $\mathbf{V}_G = -30$ to $-90\,\mathrm{V}$ straddling from n to p, and this transition can be clearly figured out in the TPNJ experiments in Fig. 2b as described earlier.

Interpretation of resistance switching of TPNJ device. According to the information on the topological surface states of both top and bottom obtained by electrical transport measurements, we can now deduce an interpretation on the experimental data on our TPNJ experiments as the following scenario shown in Fig. 2b. At $\mathbf{V}_G = 20\,\mathrm{V}$, the first TPNJ is created on the top (p-F4-TCNQ/BSTS and n-BSTS). When $\mathbf{V}_G = -30\,\mathrm{V}$ is applied as the bottom gate potential, the bottom surface of F4-TCNQ/BSTS can be tuned to p-type with leaving the both topological surface of BSTS as n-type. When $\mathbf{V}_G$ reaches $-90\,\mathrm{V}$, the bottom surface of the pristine BSTS is now tuned to a p-type, while the top surface state of BSTS remains as an n-type with bringing its chemical potential deeper into the Dirac-cone valence band on the surface. Finally, $\mathbf{V}_G = -130\,\mathrm{V}$ is applied, all topological surfaces including both the top and the bottom become p-type so

that a TPNJ can completely disappear. Consequently, the intriguing TPNJ on the entire surface (both top and bottom) conduction channel can be made only in the range of $\mathbf{V}_G$ between -30 and $-90\,\mathrm{V}$.

The simple scenario described here seems to explain our experimental observations of the sharp resistance switching in terms of an almost perfect spin-locked backward scattering between the conduction and the valence topological Dirac-cone bands created on the surface at the TPNJ. One may also wonder whether energy gap opening on the surface states due to the field induced coupling between the top and the bottom surfaces would be another scenario[41]. However, in the present experiments, we observed a clear resistance jump only at the TPNJ structure and this strongly suggests that the true scenario is TPNJ. Moreover, if the band gap opening could be the reason, one would expect that much higher bulk insulating electric resistivity could appear as the background than the present one. One remaining question is whether a sharp resistance jump can be reasonable at both the ends of TPNJ. Another possibility that other conduction channels may be involved in the switch off from the high TPNJ resistance states to the low resistance state should carefully be considered.

Analyses of the magnetoconductance using Hikami–Larkin–Nagaoka formula[33] suggested contribution of additional shallow surface accumulation layers, originating from band bending of the bulk conduction or the valence bands in pristine BSTS and F4-TCNQ/BSTS, when the theoretical interpretations[42,43] are taken into account (see Supplementary Fig. 6 and Supplementary Note 3). A similar surface accumulation layer was confirmed as a trivial band in the analysis of the SdH oscillations for F4-TCNQ/BSTS as discussed earlier. It should also be noted that a Rashba-like band[44] with π Berry phase cannot be considered because additional conduction channels suggested from the analyses of magnetoconductance are ascribed to weak localization (Berry phase ~ 0; refs 42,43).

Because exposure to the air and the moisture during the device fabrication process is known to give n-type carriers in the 3D-TIs[24,45], we assume n-type band bending for pristine BSTS (top and bottom surface) and F4-TCNQ/BSTS (bottom surface), while p-type band bending is considered in F4-TCNQ/BSTS (top surface) as shown in Fig. 4a,b. In the bottom surface, the negative $\mathbf{V}_G$ tunes the chemical potential inside the bulk band gap, resulting in the suppression of the surface accumulation layer in pristine BSTS and F4-TCNQ/BSTS, whereas it continuously tunes the chemical potential of the topological surface states to form the TPNJ shown in Fig. 4c,d. With further decrease in the $\mathbf{V}_G$, another surface accumulation layer is induced by the electric field especially at F4-TCNQ/BSTS as shown in Fig. 4e,f. Because such a conduction channel could give a sudden resistance leakage at the TPNJ leading to a low-resistant state owing to the large change in density of states of the bulk parabolic band, the surface accumulation layer could switch off the high-resistance state of TPNJ to a low resistance at $-90\,\mathrm{V}$. A similar situation occurs in the vicinity of the other perfect TPNJ junction limit at $\mathbf{V}_G = -30\,\mathrm{V}$. On the other hand, in the top surface, because p-type band bending at F4-TCNQ/BSTS continuously exists under negative $\mathbf{V}_G$ as shown in Fig. 4b,d,f, the p-type surface accumulation layer gives leakage resistance at the TPNJ. Therefore, it would contribute as a little bit broader transition rather than that at $\mathbf{V}_G = -90\,\mathrm{V}$. It is important to recognize, however, that the sharp switching in resistance occurs exactly at the both junction ends observed at $\mathbf{V}_G = -30$ and $-90\,\mathrm{V}$, where the resistance becomes maximum corresponding to the neutral point of the Dirac surface states as seen in Fig. 3g. The scenario described here on the TPNJ in 3D-TIs needs further experimental and theoretical insight in the future.
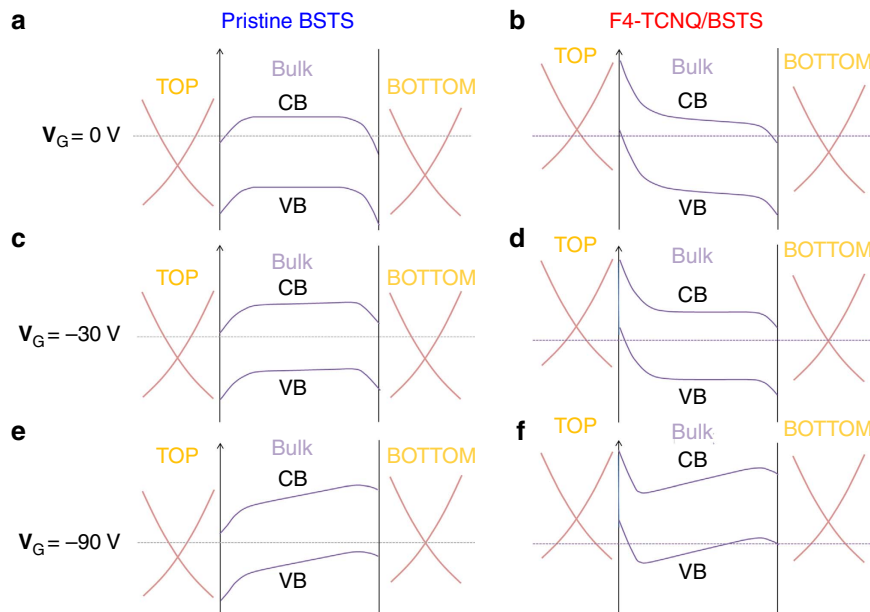
Figure 4 | Electronic structure of the present TPNJ device. The electronic structure of pristine BSTS and F4-TCNQ/BSTS in a topological p-n junction device under (**a,b**) $V_G = 0$ V, (**c,d**) $V_G = -30$ V and (**e,f**) $V_G = -90$ V. A high resistance state of TPNJ in the bottom surface can be switched on/off by tuning the chemical potential of the trivial surface accumulation layer.

Since the electronic circuit of TPNJ involving both top and bottom surfaces can be approximated as a parallel circuit connection of resistance, the equivalent electric circuit of the present device is depicted in Fig. 2c and the total resistance expected to be observed experimentally (R_{obs}) can be described by

$$1/R_{obs} = 1/[^T R_{BSTS} + {}^T R_{TPNJ} + {}^T R_{F4\text{-}TCNQ/BSTS}] + 1/[^B R_{BSTS} + {}^B R_{TPNJ} + {}^B R_{F4\text{-}TCNQ/BSTS}]$$ (2)

where $^T R$ and $^B R$ denote the resistance on the top and the bottom surfaces, respectively. R_{TPNJ} is the resistance at the TPNJ, and R_{BSTS} and $R_{F4\text{-}TCNQ/BSTS}$ are the resistances of the part of pristine BSTS and F4-TCNQ/BSTS. In the F4-TCNQ/BSTS (pristine BSTS) FET, $R_{TPNJ} = R_{BSTS} = 0$ ($R_{TPNJ} = R_{F4\text{-}TCNQ/BSTS} = 0$) is applicable to equation (2). In the F4-TCNQ/BSTS FET, the Fermi level is different between the top and the bottom surfaces due to the hole transfer from F4-TCNQ. Moreover, the trivial surface accumulation layer existing on the top surface under negative V_G may supress the ideal on/off ratio. Consequently, equation (2) gives an asymmetric structure in the $R_{xx} - V_G$ curve. In the case of pristine BSTS, the Fermi level is also different between the top and the bottom surfaces owing to the charge transfer from the substrate[46]. In addition, the n-type trivial surface accumulation layer may be suppressed under the negative V_G. Therefore, asymmetric structure in $R_{xx} - V_G$ curve with a different on/off switching ratio at both the junction ends is similarly imagined. The features given by equation (2) are qualitatively consistent with the $R_{xx} - V_G$ curves for both pristine BSTS and F4-TCNQ/BSTS as shown in Fig. 3g. When TPNJ is created on the both surfaces, high $^T R_{TPNJ}$ and $^B R_{TPNJ}$ can experimentally be expected as long as carrier conduction is prohibited by the spin locking.

According to the recent theoretical calculations[8], small but finitely non-zero transmission probability is predicted when the momentum $P_y \sim 0$, although the transmission of p-type topological surface band to n-type one, vice versa, is perfectly prohibited for the other directions. Consequently, the resistance at least one order of magnitude larger than that of the normal nn or pp connection is theoretically provided. Our present experimental values (18–27 kΩ) are smaller than such expectations (not largely different but one-third to half). One can expect $R_{obs} = [^B R_{n\text{-}BSTS} + {}^B R_{n\text{-}F4\text{-}TCNQ/BSTS}]$

for $V_G = -30$ to 20 V, and $R_{obs} = [^B R_{p\text{-}BSTS} + {}^B R_{p\text{-}F4\text{-}TCNQ/BSTS}]$ for $V_G = -130$ to -90 V. Our present experiments showed ~ 10 kΩ of $^B R_{n\text{-}BSTS} + {}^B R_{n\text{-}F4\text{-}TCNQ/BSTS}$ at $V_G = -30$ V and ~ 15 kΩ of $^B R_{p\text{-}BSTS} + {}^B R_{p\text{-}F4\text{-}TCNQ/BSTS}$, respectively and they are in good agreement with such considerations.

When one makes more quantitative discussion using the SdH oscillations and the Hall measurements, the following important messages become clear. The SdH oscillations with periodicities of $B = 16.7$ T and 43.3 T for pristine BSTS and $B = 3.55$ T and 14.5 T for F4-TCNQ/BSTS under $V_G = 0$, the carrier concentrations on the Dirac-cone surface bands can be evaluated to be 4.05×10^{11} (n) and 1.05×10^{12} cm^{-2} (n) for pristine BSTS and 8.62×10^{10} (p) and 3.52×10^{11} (n) cm^{-2} for F4-TCNQ/BSTS. One can see the clear abrupt jumps in the $R_{xx} - V_G$ in the FET output characteristics at $V_G = -30$ and -90 V due to the TPNJ on both top and bottom surfaces. One can also find similar transitions at $V_G = 20$ and -130 V, although one transmission channel becomes normal at the bottom surface with either n/n or p/p. These transitions are unfortunately not completely clear for making detailed discussion in the present experiments. By using the relative dielectric permittivity $\varepsilon_r = 3.8$ of SiO$_2$, the ideal hole number to be injected to BSTS can be evaluated to be 2.1×10^{12} and 6.3×10^{12} cm^{-2} by gating of -30 and -90 V, respectively. Considering the fact that 1.05×10^{12} (n-type carrier) cm^{-2} of n/p (B) converted to p/p (B) by $V_G = -90$ V, and from 3.52×10^{11} cm^{-2} of n/n (B) to n/p (B) at $V_G = -30$ V, the field effect for carrier accumulation is less by six to seven times than those of the ideal case. This situation seems to be strongly associated with the fact that topological nontrivial Dirac-cone surface states are created via 1:1 correspondence with the bulk and cannot be topologically separated from each other.

Comparison with previously reported TPNJ device. As for the comparison with previous report of the vertical and the in-plane TPNJ device[19–22], we did not observe the threshold-like abrupt increase of the drain current in the present drain voltage (V_D) range between -30 mV and 30 mV (ref. 22). Importantly, no clear difference was experimentally observed between positive and negative V_D, indicating that the switching of current based

on the TPNJ scenario is robust for the V_D range of the present experiments[20,22]. On the other hand, in the present device, the resistance jump at TPNJ was suppressed at 300 K (~ 26 meV) and the potential drop at TPNJ was smaller than that of the gradient induced TPNJ in the Bi_2Te_3 single crystal[21]. The Bi_2Te_3/Sb_2Te_3 heterojunction permitted the minimum film thickness of Sb_2Te_3 (15 quintuple layers) to construct a vertical TPNJ[19], a film with 10 nm (10 quintuple layers) in thickness was used to construct TPNJ in the present F4-TCNQ/BSTS device when V_G ranges from -30 to 20 V. Therefore, 3D-TI/organic molecule hybrid devices can potentially be utilized also for constructing vertical TPNJ.

Discussion

We demonstrated a switching in electrical resistance of the in-plane TPNJ fabricated on a bulk insulating BSTS ultrathin film. By using F4-TCNQ as a surface modifier, the n-type surface of BSTS thin film was successfully converted to the p-type, and the TPNJ was made on both the top and the bottom surfaces. By using accurate control of V_G in the FET structure fabricated on the transferred as-grown BSTS ultrathin film to a SiO_2/Si substrate, a sharp switching in electrical resistance was observed in four-probe resistance measurements. The present experimental results provide important clues for understanding TPNJ in 3D-TIs as well as for logical circuits made on 3D-TI materials in the future.

Methods

Growth and characterization of BSTS thin film. BSTS thin films with 10 nm film in thickness are prepared on mica by van der Waals epitaxy physical vapour deposition[26,27,47,48]. We used the $Bi_{1.5}Sb_{0.5}Te_{1.7}Se_{1.3}$ composition as the source material for the thin film crystal growth, where the surface state is tuned to n-type under the insulating bulk state[23–25]. Since the Dirac neutral point of the surface state in this composition is confirmed between the bulk valence and the conduction bands, the p-n junction on the surface states can be controlled with keeping the bulk insulating. As shown in Fig. 5, a semiconducting-like sheet resistance (R_{sheet})–
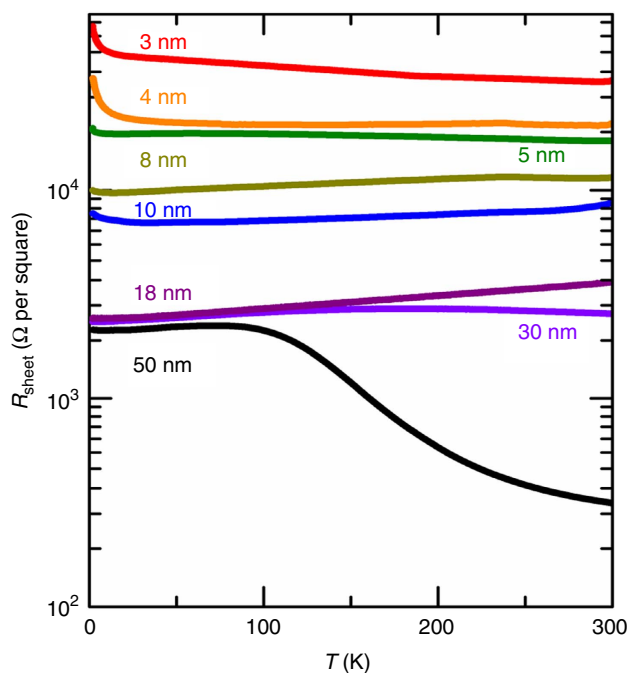

Figure 5 | Thickness dependence of electrical transport for BSTS thin films. Temperature dependence of the electrical transport for $Bi_{1.5}Sb_{0.5}Te_{1.7}Se_{1.3}$ thin film with various film thickness grown by the van der Waals epitaxy physical vapour deposition are displayed.

temperature (T) curve was observed for 50 nm thick BSTS at high temperatures due to the dominant contribution of the insulating bulk electronic states. At low temperatures, it changes to a metallic-like behaviour, being consistent with the increase in carrier mobility of the metallic surface states and the decrease in carrier numbers to be thermally populated from the bulk impurity levels. When the thickness is reduced, a semiconducting-like behaviour was suppressed even at high temperatures and a metallic behaviour became dominant when the thickness reached 10 nm. This can be understood by the fact that the contribution from the bulk states decreased due to the reduction in film thickness and the contribution of the metallic topological surface states became dominant in the total conductance in the present BSTS ultrathin films. By further decreasing the thickness of BSTS, another semiconducting-like behaviour again appears in the R_{sheet}–T curve for samples with the thickness of 4 and 3 nm. In the 3D-TIs, hybridization of the top and the bottom surfaces is expected to open an energy gap on the topological surface states when the film thickness is sufficiently thin[49]. Based on the experimental facts, the bulk electronic states of the present BSTS thin films are well insulating, and therefore the surface states reasonably give a significant contribution to the electric transport. Film thickness was determined by a surface texture measuring instrument (Surfcom 1400G—Accretech) and an atomic force microscope (AFM, SII NanoTechnology). The quality of the thin film was checked by Raman spectroscopy (Labram HR—800, Horiba, 628 nm Laser excitation). Raman spectra were acquired from the laser wavelength of 628 nm, and five peaks were observed at 109, 125, 136, 156 and 163 cm^{-1}, which are consistent with the previous results[26,27].

Device fabrication. For fabricating a back gate FET device, BSTS thin films are peeled from a mica substrate using deionized water and transferred onto a SiO_2(300 nm)/Si substrate[27]. An electrical contact was prepared by a thermal evaporation method using a metal mask (Au: 50 nm) and connected by 25 μm gold wire using silver paste (Dupont4922). F4-TCNQ was deposited on the half of a BSTS thin film by thermal evaporation under the pressure of 10^{-6} Pa to form the p-n junction on the top surface of BSTS thin films. Electrical transport measurements were performed by a standard four probe method using a semiconducting devise analyzer (Agilent B1500), a nano-voltmeter (Agilent 34420A) and a signal generator (Keithley 6221) under magnetic fields below 9 T in the temperature range of 2–300 K.

References

1. Fu, L., Kane, C. L. & Mele, E. J. Topological insulators in three dimensions. *Phys. Rev. Lett.* **98,** 106803 (2007).
2. Chen, Y. L. *et al.* Experimental realization of a three-dimensional topological insulator, Bi_2Te_3. *Science* **325,** 178–181 (2009).
3. Hsieh, D. *et al.* A tunable topological insulator in the spin helical Dirac transport regime. *Nature* **460,** 1101–1105 (2009).
4. Xia, Y. *et al.* Observation of a large-gap topological-insulator class with a single Dirac cone on the surface. *Nat. Phys* **5,** 398–402 (2009).
5. Burkov, A. A. & Hawthorn, D. G. Spin and charge transport on the surface of a topological insulator. *Phys. Rev. Lett.* **105,** 066802 (2010).
6. Wray, L. A. Device physics: topological transistor. *Nat. Phys* **8,** 705–706 (2012).
7. Wang, J., Chen, X., Zhu, B.-F. & Zhang, S.-C. Topological p-n junction. *Phys. Rev. B* **85,** 235131 (2012).
8. Habib, K. M. M., Sajjad, R. N. & Ghosh, A. W. Chiral tunneling of topological states : towards the efficient generation of spin current using spin–momentum locking. *Phys. Rev. Lett.* **114,** 176801 (2015).
9. IIan, R., de Juan, F. & Moore, J. E. Spin-based Mach-Zehnder interferometry in topological insulator p-n junctions. *Phys. Rev. Lett.* **115,** 096802 (2015).
10. Hassler, F., Akhmerov, A. R. & Beenakker, C. W. J. Flat – lens focusing of electrons on the surface of a topological insulator. *Phys. Rev. B* **82,** 125423 (2010).
11. Yamakage, A., Imura, K-I., Cayssol, J. & Kuramoto, Y. Interfacial charge and spin transport in Z_2 topological insulators. *Phys. Rev. B* **83,** 125401 (2011).
12. Mellnik, A. R. *et al.* Spin-transfer torque generated by a topological insulator. *Nature* **511,** 449–451 (2014).
13. Shiomi, Y. *et al.* Spin-electricity conversion induced by spin injection into topological insulators. *Phys. Rev. Lett.* **113,** 196601 (2014).
14. Maciejko, J., Kim, E.-A. & Qi, X.-L. Spin Aharonov - Bohm effect and topological spin transistor. *Phys. Rev. B* **82,** 195409 (2010).
15. Huard, B. *et al.* Transport measurements across a tunable potential barrier in graphene. *Phys. Rev. Lett.* **98,** 236803 (2007).
16. Williams, J. R., DiCarlo, L. & Marcus, C. M. Quantum Hall effect in a gate-controlled p-n junction of graphene. *Science* **317,** 638–641 (2007).
17. Ozyilmaz, B. *et al.* Electronic transport and quantum Hall effect in bipolar graphene p-n-p junctions. *Phys. Rev. Lett.* **99,** 166804 (2007).
18. Mi, J.-L. *et al.* Phase separation and bulk p-n transition in single crystals of Bi_2Te_2Se topological insulator. *Adv. Mater.* **25,** 889–893 (2013).

19. Eschbach, M. *et al.* Realization of a vertical topological p-n junction in epitaxial Sb_2Te_3/Bi_2Te_3 heterostructures. *Nat. Commun.* **6,** 8816 (2015).

20. Li, Y. *et al.* Lateral and vertical two-dimensional layered topological insulator heterostructure. *ACS Nano* **9,** 10916–10921 (2015).

21. Bathon, T. *et al.* Experimental realization of a topological p-n junction by intrinsic defect-grading. *Adv. Mater.* **28,** 2183–2188 (2016).

22. Fei, F. *et al.* Solvothermal synthesis of lateral heterojunction Sb_2Te_3/Bi_2Te_3 nanoplates. *Nano Lett.* **15,** 5905–5911 (2015).

23. Ren, Z., Taskin, A. A., Sasaki, S., Segawa, K. & Ando, Y. Optimizing $Bi_{2-x}Sb_xTe_{3-y}Se_y$ solid solutions to approach the intrinsic topological insulator regime. *Phys. Rev. B* **84,** 165311 (2011).

24. Taskin, A. A., Ren, Z., Sasaki, S., Segawa, K. & Ando, Y. Observation of Dirac holes and electrons in a topological insulator. *Phys. Rev. Lett.* **107,** 016801 (2011).

25. Arakane, T. *et al.* Tunable Dirac cone in the topological insulator $Bi_{2-x}Sb_xTe_{3-y}Se_y$. *Nat. Commun.* **3,** 636 (2012).

26. Tu, N. H. *et al.* Van der Waals epitaxial growth of topological insulator $Bi_{2-x}Sb_xTe_{3-y}Se_y$ ultrathin nanoplate on electrically insulating fluorophlogopite mica. *Appl. Phys. Lett.* **105,** 063104 (2014).

27. Tu, N. H., Tanabe, Y., Satake, Y., Huynh, K. K. & Tanigaki, K. Large-area and transferred high-quality three-dimensional topological insulator $Bi_{2-x}Sb_xTe_{3-y}Se_y$ ultrathin film grown by catalyst-free physical vapor deposition. Preprint at https://arxiv.org/abs/1601.06541 (2016).

28. Kim, D. *et al.* Surface conduction of topological Dirac electrons in bulk insulating Bi_2Se_3. *Nat. Phys.* **8,** 459–463 (2012).

29. Tanabe, Y. *et al.* Electron and hole injection via charge transfer at the topological insulator $Bi_{2-x}Sb_xTe_{3-y}Se_y$ organic molecule interface. *J. Phys. Chem. C* **118,** 3533–3538 (2014).

30. Wang, J. *et al.* Molecular doping control at a topological insulator surface: F4-TCNQ on Bi_2Se_3. *J. Phys. Chem. C* **118,** 14860–14865 (2014).

31. Wu, L. *et al.* Tuning and stabilizing topological insulator Bi_2Se_3 in the intrinsic regime by charge extraction with organic overlayers. *Appl. Phys. Lett* **108,** 221603 (2016).

32. Gao, W. Y. & Kahn, A. Controlled p doping of the hole-transport molecular material N,N′-diphenyl-N,N′-bis(1-naphtyl)-1,1′-biphenyl-4,4′-diamine with tetrafluorotetracyanoquinodimethane. *J. Appl. Phys.* **94,** 359–366 (2003).

33. Hikami, S., Larkin, A. I. & Nagaoka, Y. Spin – orbit interaction and magnetoresistance in the two – dimensional random system. *Prog. Theor. Phys.* **63,** 707–709 (1980).

34. Sessi, P., Bathon, T., Kokh, K. A., Tereshchenko, O. E. & Bode, M. Probing the electronic properties of individual MnPc molecules coupled to topological states. *Nano Lett.* **14,** 5092–5096 (2014).

35. Bathon, T., Sessi, P., Kokh, K. A., Tereshchenko, O. E. & Bode, M. Systematics of molecular self-assembled networks at topological insulators surfaces. *Nano Lett.* **15,** 2442–2447 (2015).

36. Taskin, A. A., Sasaki, S., Segawa, K. & Ando, Y. Manifestation of topological protection in transport properties of epitaxial Bi_2Se_3 thin films. *Phys. Rev. Lett.* **109,** 066803 (2012).

37. Ando, Y. Topological insulating materials. *J. Phys. Soc. Jpn* **82,** 102001 (2013).

38. Jakobs, S. *et al.* Controlling the spin texture of topological insulators by rational design of organic molecules. *Nano Lett.* **15,** 6022–6029 (2015).

39. Shen, S. Q. Spin Hall effect and Berry phase in two-dimensional electron gas. *Phys. Rev. B* **70,** 081311 (2004).

40. Xu, Y. *et al.* Observation of topological surface state quantum Hall effect in an intrinsic three–dimensional topological insulator. *Nat. Phys.* **10,** 956–963 (2014).

41. Fatemi, V. *et al.* Electrostatic coupling between two surfaces of a topological insulator nanodevice. *Phys. Rev. Lett.* **113,** 2006801 (2014).

42. Lu, H. Z. & Shen, S. Q. Weak localization of bulk channels in topological insulator thin films. *Phys. Rev. B* **84,** 125138 (2011).

43. Garate, I. & Glazman, L. Weak localization and antilozalization in topological insulator thin films with coherent bulk-surface coupling. *Phys. Rev. B* **86,** 035422 (2012).

44. Yang, F. *et al.* Switching of charge-current-induced spin polarization in the topological insulator $BiSbTeSe_2$. *Phys. Rev. B* **94,** 075304 (2016).

45. Kong, D. *et al.* Rapid surface oxidation as a source of surface degradation factor for Bi_2Se_3. *ACS Nano* **5,** 4698–4703 (2011).

46. Veyrat, L. *et al.* Band bending inversion in Bi_2Se_3 nanostructures. *Nano Lett.* **15,** 7503–7507 (2015).

47. Li, H. *et al.* Controlled synthesis of topological insulator nanoplate arrays on mica. *J. Am. Chem. Soc.* **134,** 6132–6135 (2012).

48. Jing, Y. *et al.* Weak antilocalization and electron–electron interaction in coupled multiple channel transport in a Bi_2Se_3 thin film. *Nanoscale* **8,** 1879–1885 (2016).

49. Zhang, Y. *et al.* Crossover of the three-dimensional topological insulator Bi_2Se_3 to the two-dimensional limit. *Nat. Phys.* **6,** 584–588 (2010).

Author contributions

Y.T., K.T. designed the project. N.H.T, Y.T. and Y.S. synthesized $Bi_{2-x}Sb_xTe_{3-y}Se_y$ (BSTS) thin film by the van deer Waals epitaxy and fabricated BSTS p-n junction device. N.H.T., Y.T. characterized BSTS thin films. N.H.T., Y.T. and K.K.H. measured BSTS p-n junction devices. N.H.T., Y.T. and K.T. wrote a manuscript. All the authors discussed the results and commented on the manuscript.

Additional information

Supplementary Information accompanies this paper at http://www.nature.com/naturecommunications

Competing financial interests: The authors declare no competing financial interests.

Reprints and permission information is available online at http://npg.nature.com/reprintsandpermissions/

How to cite this article: Tu, N. H. *et al.* In-plane topological p-n junction in the three-dimensional topological insulator $Bi_{2-x}Sb_xTe_{3-y}Se_y$. *Nat. Commun.* **7,** 13763 doi: 10.1038/ncomms13763 (2016).

Publisher's note: Springer Nature remains neutral with regard to jurisdictional claims in published maps and institutional affiliations.